Extension of the Deflection-Domain Passivity Approach for Variable Stiffnesses to SO(3)

Michael Panzirsch[1], Harsimran Singh[1,2], Marek Sierotowicz[1,3], Alexander Dietrich[1]

***Abstract*—Recently, the deflection-domain passivity approach (DDPA) was introduced which does not control a system's energetic behavior over time but over the deflection of the coupling controller's virtual spring. So far, it has been applied to guarantee passivity in variable stiffness systems and for chattering-free force attenuation. When compared to time-domain based approaches as the Time Domain Passivity Approach or energy-tanks, the DDPA yields a more continuous and proactive variation of the controller force since the required dissipative action is distributed over the deflection of the spring applied in the coupling controller. In contrast, time-based approaches behave non-proactively and often attenuate control signals such as commanded forces completely. This attenuation happens suddenly when no energy is left available with regards to passivity. The DDPA was the first method to ensure passivity and non-zero stiffnesses for arbitrary unknown stiffness profiles. Here, we extend the DDPA to the control of three energetically coupled rotations in SO(3). Experiments in a teleoperation setup confirm the functionality of the approach.**

***Index Terms*—Variable Impedance, Telerobotics and Teleoperation, Deflection-Domain Passivity Approach**

I. Introduction

THE passivity criterion is one of the most commonly used principles for system design and analysis in robotics. Passive control circuits can be achieved through passive system design in the frequency-domain using, for instance, the Raisbeck criterion or through time-domain based approaches such as the Time-Domain Passivity Approach (TDPA, [1], [2]) or energy tanks [3], [4], [5]. Frequency-based control mostly leads to conservative control actions due to its non-adaptive nature. Time-domain based approaches on the other hand, provide less conservative adaptive damping mainly through variation of control commands such as forces or velocities. Still, the dissipative action happens suddenly in a non-predictive manner when the energy storage is empty and passivity would be violated otherwise. Thereby, the control forces may be completely attenuated leading to zero-stiffness phases in the impedance controller [6]. Such coupling controllers penalize a deviation between desired and actual pose with spring-like characteristics. Especially in passivity-based control of variable stiffnesses [3], [7], [5], [2], such periods are probable and represent an undesired behavior. Robots with such software or hardware-based [8], [9], [10] variable impedance promise a high degree of safety in human-robot shared environments while featuring a high positioning accuracy and the ability to handle heavy loads. In EMG-based tele-impedance [2], a human can adapt the compliance of the teleoperated robot by varying his/her arm stiffness.

In the majority of passivity-based methods for variable stiffnesses, adequate design of the stiffness variation is required to avoid zero-stiffness phases. Therefore, in [11], we proposed the passivity-based control in the deflection domain (Deflection-Domain Passivity Approach, DDPA, Patent DE102021111413B3) referring to the deflection of the virtual spring of the coupling controller inspired by [12], [13].

In simplified terms, the spring stiffness is limited on the releasing path (maximum to zero deflection) by the DDPA in a way such that the available energy (measured in time-domain) becomes zero at zero deflection, thus ensuring passivity. Thus, the controller force is adapted continuously and earlier than in time-based methods such that phases of complete attenuation of the control command can be avoided. In [11], the DDPA was compared with the energy-reflection based TDPA (TDPA-ER, [14]) leading to zero-stiffness phases in contrast to DDPA. The DDPA was later applied in delayed teleoperation setups for continuous energy dissipation independent of variable stiffnesses to increase the force transparency of the TDPA-ER [15]. The respective extension to the 6-DoF TDPA-ER implementation [16] requires the DDPA method proposed in the present work. The DDPA inspired the error-domain conservativity control recently introduced for haptics in [17].

The DDPA can be applied to ensure passivity in systems applying a spatial coupling controller such that a coupling stiffness can be varied. Thereby, the DDPA can especially replace comparable methods that attenuate the force command directly. This holds for, but is not limited to, variable stiffness control and delayed teleoperation or tele-impedance [2].

The DDPA has been only applied on translational degrees of freedom (DoF) so far. To enable robotics with entirely variable compliance, the extension to 6-DoF is required. Since translations can be controlled separately with DDPA, only the extension to SO(3) remains. In contrast to translations,

Manuscript received: July 28, 2023; Revised: November 23, 2023; Accepted: January 14, 2024. This paper was recommended for publication by Editor Jee-Hwan Ryu upon evaluation of the Associate Editor and Reviewers' comments. The work was partially funded by the Bavarian Ministry of Economic Affairs, Regional Development and Energy, within the project SMiLE2gether (LABAY102). The research work was partially funded by the German Research Foundation (DFG, Deutsche Forschungsgemeinschaft) as part of Germany's Excellence Strategy – EXC 2050/1 – Project ID 390696704 – Cluster of Excellence "Centre for Tactile Internet with Human-in-the-Loop" (CeTI) of Technische Universität Dresden.

[1] M. Panzirsch, H. Singh, M. Sierotowicz and A. Dietrich are with the Institute of Robotics and Mechatronic, German Aerospace Center (DLR), Wessling, Germany. michael.panzirsch@dlr.de

[2] H. Singh is with the Centre for Tactile Internet with Human-in-the-Loop (CeTI), Cluster of Excellence at TU Dresden, Dresden, Germany.

[3] M. Sierotowicz is with the Chair of Assistive Intelligent Robotics, Department for Artificial Intelligence in Biomedical Engineering, Friedrich Alexander Universität Erlangen-Nürnberg, 91052 Erlangen, Germany.

Digital Object Identifier (DOI): see top of this page.

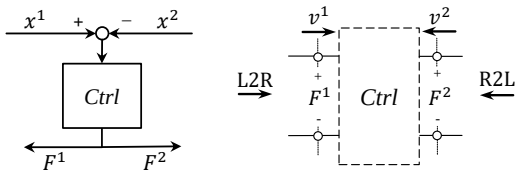

(a) Signal flow diagram. (b) Network representation.

Fig. 1: Coupling controller [11].

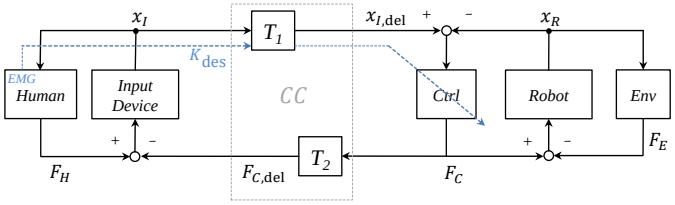

Fig. 2: Signal flow diagram for delayed tele-operation with variable stiffness K_{des} [11].

rotational DoF are coupled, i.e. energy injected in one rotational DoF may be extracted in another DoF in the task space. Therefore, rotations have to be controlled conjointly since they require one common energy storage for passivity-based control. Here, we propose a solution of the DDPA framework for rotational DoF based on the angle-axis representation for intrinsically passive controllers [18]. We restrict spatial springs to such without coupling between translations and rotations.

The paper is structured as follows: Section II presents the fundamentals of the DDPA. Section III introduces the proposed approach, followed by simulations in Section IV and an experimental evaluation in Section V. Finally, Section VI summarizes the results and concludes the work.

II. Fundamentals

A. The 1-DoF DDPA

The control principle of the DDPA involving energy observation over time and stiffness limitation over the spring deflection was introduced in [11]. Fig. 1 presents the control signal flow diagram and the respective network representation of a virtual spring ($Ctrl$) coupling for instance input device and robot as depicted in Fig. 2. In such teleoperation setups, a $Human$ operator controls the $Robot$ motion in its environment (Env) via an $Input\ Device$. The commanded motion x_I may be delayed by T_1 and the feedback of the controller force F_c displayed on the $Input\ Device$ may be delayed by T_2. Using sEMG on the operator's forearm (similarly to [11]), the desired stiffness K_{des} can be estimated and applied in $Ctrl$ representing a tele-impedance setup [2].

In [11] it was shown how the DDPA can ensure passivity in case of arbitrary stiffness profiles while avoiding zero stiffness phases. At port 1 and 2 of Fig. 1b, the energy input and output can be observed over time with the effort (force) F^i and flow (velocity) v^i at port i.

$$P^i_{\text{L2R}}(k) = \begin{cases} 0, & \text{if } P^i(k) < 0, \\ P^i(k), & \text{if } P^i(k) > 0, \end{cases} \tag{1}$$

$$P^i_{\text{R2L}}(k) = \begin{cases} 0, & \text{if } P^i(k) > 0, \\ -P^i(k), & \text{if } P^i(k) < 0, \end{cases} \tag{2}$$

with the power $P^i(k) = F^i(k)v^i(k)$ at time step k. The power P^i_{L2R} flows in left-to-right direction and the power P^i_{R2L} in right-to-left direction at port i. The flow direction can be distinguished by the sign of the power which also depends on the sign convention of the controller $Ctrl$. The respective energies E^i_{L2R} and E^i_{R2L} (positive by definition) can be computed via discrete time integration ($E^i(k) = \sum_{j=0}^{k} P^i(j)T_s$, with sampling time T_s).

The current energy content of $Ctrl$ (consisting mainly of potential energy of the spring) can be determined from the in- and outgoing energies of the $Ctrl$ 1-port:

$$\begin{aligned} E_{\text{obs}}(k) = E^1_{\text{L2R}}(k) + E^2_{\text{R2L}}(k) \\ - E^1_{\text{R2L}}(k) - E^2_{\text{L2R}}(k). \end{aligned} \tag{3}$$

As discussed in detail in [11], for certain stiffness profiles (e.g. constantly increasing stiffness) over the spring deflection δ, the energy E_{obs} will become negative indicating energy generation (non-passive behavior). Thereby, energy is injected during the pressing (or pulling) part of a spring deflection phase (spring extension) and ejected during the releasing part respectively. At each arbitrary maximum deflection of the spring $\delta_{\max}$, the DDPA yields a limiting stiffness profile K_{lim} for the release path to ensure passivity. For simple stiffness variations during the pressing phase, the limiting stiffness function can be linear. If too low stiffnesses result from K_{lim} (compare Fig. 3), the stiffness may already be limited on the pressing path and polynomial limiting functions can be applied. The value K_{init} is the stiffness at the start of a deflection phase, and $K_{\min}$ is the minimally acceptable stiffness. From here, the spring deflection δ refers to its absolute value $|\delta|$ for the sake of simplicity. The reader is referred to [11] for more details.

The polynomial K_{lim} derived for translational DoF in [11] is:

$$\begin{aligned} K_{\text{lim}}(\delta) = \frac{K_{k1} - K_{\text{init}} - \frac{3E_{\text{obs}}(\delta_{k1})}{\delta^2_{k1}} + \frac{3K_{\text{init}}}{2}}{\delta^d_{k1}(1 - \frac{3}{d+2})}\delta^d \\ + \frac{E_{\text{obs}}(\delta_{k1}) - \frac{a}{d+2}\delta^{d+2}_{k1} - \frac{K_{\text{init}}}{2}\delta^2_{k1}}{\frac{1}{3}\delta^3_{k1}}\delta + K_{\text{init}}, \end{aligned} \tag{4}$$

with

$$a = \frac{K_{k1} - c - \frac{3E_{\text{obs}}(\delta_{k1})}{\delta^2_{k1}} + \frac{3c}{2}}{\delta^d_{k1}(1 - \frac{3}{d+2})}, \tag{5}$$

and polynomial exponent d. The value c can be set to K_{init} and $k1$ denotes the time step at which the function K_{lim} is calculated. In [11], K_{lim} was derived from $E_{\text{obs}}(\delta)$

$$\begin{aligned} E_{\text{obs}}(\delta) &= \int_0^{\delta} K_{\text{lim}}(\xi)\xi d\xi \\ &= a\frac{1}{d+2}\delta^{d+2} + b\frac{1}{3}\delta^3 + c\frac{1}{2}\delta^2, \end{aligned} \tag{6}$$

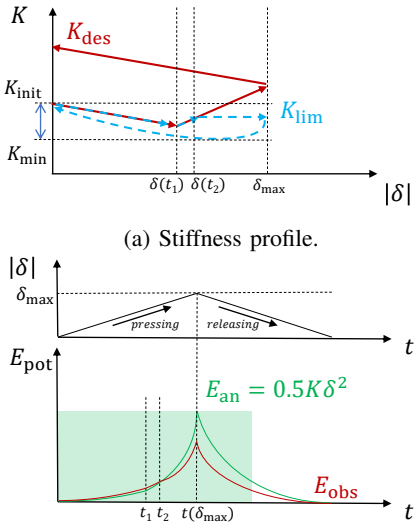

(a) Stiffness profile.

(b) Potential energies.

Fig. 3: Passivity-based control with polynomial limiting function $K_{\text{lim}}^{\text{pol}}$ with stiffness limitation during pressing path (adapted from [11]).

based on the exemplary polynomial function $K_{\text{lim}}(\delta) = a\delta^d + b\delta + c$.

The described 1-DoF case can be easily extended to three translations since they can be regarded separately with three independent energy storages. Here, we concentrate on the extension to the SO(3) rotation group which is not straight forward in contrast since the rotational DoF are coupled energetically and kinematically.

B. Spatial Springs

The spatial springs with translational and orientational stiffness components of [18], [19] produce a computed wrench $\boldsymbol{\omega}_c$

$$\boldsymbol{\omega}_c = \begin{pmatrix} \boldsymbol{\tau}_c \\ \mathbf{f}_c \end{pmatrix}, \tag{7}$$

with torques $\boldsymbol{\tau}_c$ and forces $\mathbf{f}_c$. The overall power at port i in the rotational DoF d can be calculated as

$$P^{\text{rot},i}(k) = \sum_{d=1}^{3} \tau_{c,d}^{i}(k)\nu_d^i(k), \tag{8}$$

with the angular velocity $\boldsymbol{\nu}$. Note that power that enters in one DoF may exit in another DoF such that P^{rot} has to be observed in sum. The flow direction of the power (L2R, R2L) can be determined analogous to (1) and (2). The energy $E_n^{\text{rot},i}(k)$ at port i is calculated via integration of the respective power: $E_n^{\text{rot},i}(k) = \sum_{j=0}^{k} P_n^{\text{rot},i}(j)T_s$, with sampling time T_s and $n \in \{\text{L2R}, \text{R2L}\}$.

Based on the direction specific energy values $E_{L2R}^{rot,i}$ and $E_{R2L}^{rot,i}$, the storage of available energy $E_{\text{obs}}^{\text{rot}}$ can be found as:

$$\begin{aligned} E_{\text{obs}}^{\text{rot}}(k) = E_{\text{L2R}}^{\text{rot},1}(k) + E_{\text{R2L}}^{\text{rot},2}(k) \\ - E_{\text{R2L}}^{\text{rot},1}(k) - E_{\text{L2R}}^{\text{rot},2}(k). \end{aligned} \tag{9}$$

The input to spatial springs is the spatial distance ${}^{\mathcal{D}}\mathbf{H}_{\mathcal{T}}$ between reference frame ${}^{\mathcal{W}}\mathbf{H}_{\mathcal{D}}$ and the robot tool frame ${}^{\mathcal{W}}\mathbf{H}_{\mathcal{T}}$ defined in the world frame $\mathcal{W}$:

$${}^{\mathcal{D}}\mathbf{H}_{\mathcal{T}} = \begin{pmatrix} {}^{\mathcal{D}}\mathbf{R}_{\mathcal{T}} & {}^{\mathcal{D}}\mathbf{p}_{\mathcal{T}} \\ 0 & 1 \end{pmatrix}, \tag{10}$$

with ${}^{\mathcal{D}}\mathbf{R}_{\mathcal{T}}$, the SO(3) element of ${}^{\mathcal{D}}\mathbf{H}_{\mathcal{T}}$, and the translation ${}^{\mathcal{D}}\mathbf{p}_{\mathcal{T}}$ between the two frames $\mathcal{D}$ and $\mathcal{T}$. To enable the application of DDPA, the rotation matrix ${}^{\mathcal{D}}\mathbf{R}_{\mathcal{T}}$ will be simplified to the angle-axis representation with axis ${}^{\mathcal{D}}\mathbf{r}_{\mathcal{T}}$ and angle ${}^{\mathcal{D}}\Theta_{\mathcal{T}}$. According to [20], the angle ${}^{\mathcal{D}}\Theta_{\mathcal{T}}$ is calculated from ${}^{\mathcal{D}}\mathbf{H}_{\mathcal{T}}$ via the trace tr of the rotation matrix ${}^{\mathcal{D}}\mathbf{R}_{\mathcal{T}}$

$${}^{\mathcal{D}}\Theta_{\mathcal{T}} = \arccos\left(\frac{\text{tr}({}^{\mathcal{D}}\mathbf{R}_{\mathcal{T}}) - 1}{2}\right). \tag{11}$$

The normalized axis ${}^{\mathcal{D}}\mathbf{r}_{\mathcal{T}}$ of the angle-axis representation can be found as

$${}^{\mathcal{D}}\mathbf{r}_{\mathcal{T}} = \frac{1}{2\sin\Theta}\begin{bmatrix} {}^{\mathcal{D}}R_{\mathcal{T}}(3,2) - {}^{\mathcal{D}}R_{\mathcal{T}}(2,3) \\ {}^{\mathcal{D}}R_{\mathcal{T}}(1,3) - {}^{\mathcal{D}}R_{\mathcal{T}}(3,1) \\ {}^{\mathcal{D}}R_{\mathcal{T}}(2,1) - {}^{\mathcal{D}}R_{\mathcal{T}}(1,2) \end{bmatrix}. \tag{12}$$

Figure 4 visualizes the angle-axis representation of rotations and the application of DDPA to SO(3) introduced in the following.

In robotics, 1-DoF rotational springs with nonlinear stiffness $k^{\text{nl}} = k_o\cos(\Theta)$ (with $[k_0]{=}\frac{Nm}{rad}$, [18], [21], [22]) are applied to achieve a continuous spring torque $\tau^{\text{nl}} = k_o\sin(\Theta)$ at high spring deflections on $[0, 2\pi]$.

Proposition 1: Integrating the 1-DoF spring torque τ^{nl} over the spring deflection Θ, the analytical potential energy $V_{\text{an}}^{\text{nl}}$ results in:

$$V_{\text{an}}^{\text{nl}}(\Theta, \mathbf{r}) = \int_0^{\Theta} \tau^{\text{nl}}(x)dx = 2k_0\sin^2\frac{\Theta}{2}. \tag{13}$$

With the stiffness matrix ${}^{\mathcal{D}}\mathbf{K}_o$ defined in the desired robot frame $\mathcal{D}$, the torque vector in SO(3) becomes $\tau^{\text{nl}} = {}^{\mathcal{D}}\mathbf{r}_{\mathcal{T}}^T\,{}^{\mathcal{D}}\mathbf{K}_o\,{}^{\mathcal{D}}\mathbf{r}_{\mathcal{T}} sin({}^{\mathcal{D}}\Theta_{\mathcal{T}})$. The analytical potential energy of spatial springs in SO(3) becomes:

$$\begin{aligned} V_{\text{an}}^{\text{nl}}(\Theta, \mathbf{r}) &= \int_0^{{}^{\mathcal{D}}\Theta_{\mathcal{T}}} ({}^{\mathcal{D}}\mathbf{r}_{\mathcal{T}}^T\,{}^{\mathcal{D}}\mathbf{K}_o\,{}^{\mathcal{D}}\mathbf{r}_{\mathcal{T}} sin(x))dx \\ &= (1 - cos({}^{\mathcal{D}}\Theta_{\mathcal{T}}))\,{}^{\mathcal{D}}\mathbf{r}_{\mathcal{T}}^T\,{}^{\mathcal{D}}\mathbf{K}_o\,{}^{\mathcal{D}}\mathbf{r}_{\mathcal{T}}. \end{aligned} \tag{14}$$

Applying trigonometric rules, $V_{\text{an}}^{\text{nl}}$ can be simplified to:

$$V_{\text{an}}^{\text{nl}}(\Theta, \mathbf{r}) = 2\sin^2\left(\frac{{}^{\mathcal{D}}\Theta_{\mathcal{T}}}{2}\right){}^{\mathcal{D}}\mathbf{r}_{\mathcal{T}}^T\,{}^{\mathcal{D}}\mathbf{K}_o\,{}^{\mathcal{D}}\mathbf{r}_{\mathcal{T}}. \tag{15}$$

From this equation, the influence of the scalar angle ${}^{\mathcal{D}}\Theta_{\mathcal{T}}$ and the axis ${}^{\mathcal{D}}\mathbf{r}_{\mathcal{T}}$ on the potential energy can be well analyzed.

III. Proposed Method

To transfer the DDPA with the two scalar control variables δ and K_{lim} from 1-DoF to SO(3), a suitable representation for the rotational spring deflection and stiffness needs to be defined. Direct control of the various components of the stiffness matrix is not feasible since the energy term would depend on more than one scalar control variable. In order to

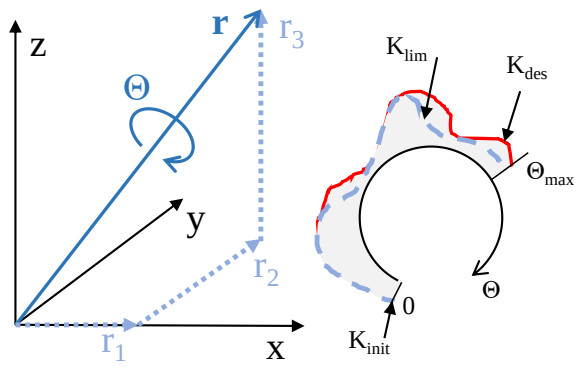

Fig. 4: Angle-axis representation and DDPA for SO(3). *Left:* Angle Θ and axis $\mathbf{r}$ with components r_1,r_2, and r_3. *Right:* Stiffness variation over the deflection of the spatial spring represented by the angle Θ.

apply DDPA to all three rotational DoF conjointly, we propose to consider the scalar angle Θ (again as absolute value) of the angle-axis representation as the deflection δ of the DDPA.

A. 6-DoF DDPA concept

For ease of understanding, we first introduce a simplified case limited to a diagonal stiffness matrix with uniform diagonal entries:

Method M1 *- Diagonal stiffness matrix with uniform diagonal entries:* An essential aspect for DDPA in the rotational DoF is the energy injection or dissipation of $V_{\mathrm{an}}^{\mathrm{nl}}$ (15) when the orientation of the axis $\mathbf{r}$ changes. I.e., the energy ejection during the release phase of the spatial spring does not exclusively depend on $\delta{=}\Theta$ but also on the variation of $\mathbf{r}$. To simplify the DDPA design, we first consider a $\mathbf{K}_{\mathrm{o}}$ that renders $V_{\mathrm{an}}^{\mathrm{nl}}$ solely dependent on Θ. Therefore, we formulate the following theorem:

Theorem 1: We define s_{des} ([-]) as the desired and potentially variable stiffness scaling. Then, a spatial spring with diagonal stiffness matrix and uniform diagonal entries ${}^{\mathcal{D}}\mathbf{K}_{\mathrm{o}}(\Theta) = s_{\mathrm{des}}(\Theta)k_0\mathbf{I}$ behaves energy-conserving (lossless) when the axis $\mathbf{r}$ of orientation is varied. Thus, the DDPA can be applied to limit the desired stiffness scaling s_{des} to s_{lim}. Note that the finally applied stiffness scaling is $s_{\mathrm{act}}{=}\min(s_{\mathrm{lim}}, s_{\mathrm{des}})$.

This theorem is proven in the following:

Lemma 1: Since the axis of the angle-axis representation ${}^{\mathcal{D}}\mathbf{r}_{\mathcal{T}}$ is of unit length ($|{}^{\mathcal{D}}\mathbf{r}_{\mathcal{T}}| = 1$), the following holds:

$$ {}^{\mathcal{D}}\mathbf{r}_{\mathcal{T}}^{T}\,{}^{\mathcal{D}}\mathbf{r}_{\mathcal{T}} = |{}^{\mathcal{D}}\mathbf{r}_{\mathcal{T}}|^2 = 1. \tag{16}$$

Proof 1: We choose a diagonal stiffness matrix ${}^{\mathcal{D}}\mathbf{K}_{o}$ such that ${}^{\mathcal{D}}\mathbf{K}_{\mathrm{o}}(\Theta){=}k_0 s_{\mathrm{act}}(\Theta)\mathbf{I}$. Then, with Lemma 1, the influence of $\mathbf{r}$ vanishes and $V_{\mathrm{an}}^{\mathrm{nl}}(k)$ can be derived analogous to (13).

Since the DDPA controlled variable s_{act} is a scalar, the polynomial s_{lim} can be found analogous to the 1-DoF case. Note that these equations serve the passivity control, but that energy needs to be observed over time according to (9).

Method M2 *- Arbitrary stiffness matrices:* The scalar scaling $s_{\mathrm{act}}(\Theta)$ of a stiffness matrix ${}^{\mathcal{D}}\mathbf{K}_{\mathrm{o}}$ can also be applied as the single DDPA control variable in case of stiffness matrices ${}^{\mathcal{D}}\mathbf{K}_{\mathrm{o}}^{*}$ with non-uniform components:

$$ {}^{\mathcal{D}}\mathbf{K}_{\mathrm{o}} = s_{\mathrm{act}}({}^{\mathcal{D}}\Theta_{\mathcal{T}})\,{}^{\mathcal{D}}\mathbf{K}_{\mathrm{o}}^{*}. \tag{17}$$

Applying (17) to the integral of (14), the polynomial s_{lim} can be found analogous to the 1-DoF case. Then, with (17) and $\tau^{\mathrm{nl}} = {}^{\mathcal{D}}\mathbf{r}_{\mathcal{T}}^{T}\,{}^{\mathcal{D}}\mathbf{K}_{o}\,{}^{\mathcal{D}}\mathbf{r}_{\mathcal{T}} sin({}^{\mathcal{D}}\Theta_{\mathcal{T}})$ the polynomial s_{lim} becomes:

$$ s_{lim}(\delta) = \frac{(E_{obs} - K_0)\delta_{k1} - (K_{k1} - K_0)s_{k1} + K_{k1}\delta_{k1}c_{k1}}{2(c_{k1}-1)\delta_{k1} + s_{k1}\delta_{k1}^2}\delta^2 + \frac{(E_{obs} + K_0(c_{k1}-1) + f)}{(s_{k1} - \delta_{k1}c_{k1})}\delta + K_0 $$

with $f = \frac{((c_{k1}(\delta_{k1}^2-2)-2\delta_{k1}s_{k1}+2)g)}{(2\delta_{k1}c_{k1}-2\delta_{k1}+\delta_{k1}^2 s_{k1})}$, $s_{k1} = sin(\delta_{k1})$, $g = (E_{obs} - K_0 + K_{k1}c_{k1})\delta_{k1} - (K_{k1} - K_0)s_{k1}$, and $c_{k1} = cos(\delta_{k1})$. Note that with ${}^{\mathcal{D}}\mathbf{r}_{\mathcal{T}}$ a time-varying element remains in the energy terms besides the state variable Θ. Therefore, the observed energy E_{obs} may increase or decrease due to changes in $\mathbf{r}$, even while Θ may remain constant. Still, the passivity w.r.t. a non-variable spatial spring is guaranteed since for a variation of $\mathbf{r}$ energy needs to be injected or ejected resulting in a lossless spring behavior. In DDPA, the presence of an additional time-varying influence has to be accounted for as follows:

- In contrast to the 1-DoF implementation of DDPA, in case of arbitrary stiffness matrices, the polynomial limiting function s_{lim} has to be recalculated in each time step. This is due to the fact that through the variation of $\mathbf{r}$, energy can be injected or released from the coupling controller which needs to be considered in the DDPA.
- The scalar value

$$ u(t) = {}^{\mathcal{D}}\mathbf{r}_{\mathcal{T}}^{T}(t)\,{}^{\mathcal{D}}\mathbf{K}_{\mathrm{o}}^{*}\,{}^{\mathcal{D}}\mathbf{r}_{\mathcal{T}}(t) \tag{18}$$

  is considered in the polynomial stiffness equation (4) via

$$ E_{\mathrm{obs}}^{*}(t) = E_{\mathrm{obs}}(t)/u(t). \tag{19}$$

  This division by u annihilates the effect of the axis ${}^{\mathcal{D}}\mathbf{r}_{\mathcal{T}}$ in the observed energy such that $K_{\mathrm{lim}}(\Theta)$ (compare (4)) depends solely on the time-dependent variable Θ.

B. Implementation

The signal flow diagram of Fig. 5 presents the proposed implementation of the 6-DoF DDPA. Note that the variation of $\mathbf{r}$ is assumed to be negligible in the numerical differentiation step. Analogous to the translational DDPA of [11], the following aspects of implementation are recommended.

- *Deflection deadband:* For the sake of robustness, a minimum absolute spring deflection value $|\Theta_{\mathrm{db}}|$ should be chosen to ensure robustness due to singularities. It has already been confirmed in [11] that no relevant energy generation results from such deadbands. Within this deadband, s_{act} is set to s_{des} and the observed energy is reset to zero.
- *Filter:* The detection of a releasing and pressing phase can be filtered for increased robustness. Here, we account for a change between the phases if the change was of minimum amplitude and preserved for a minimum time.

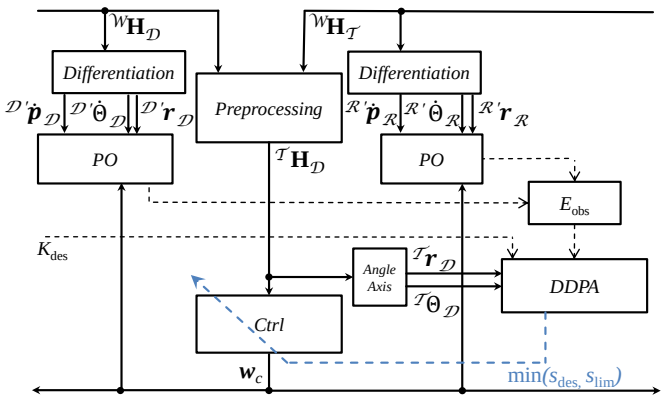

Fig. 5: Signal flow diagram of the proposed 6DoF DDPA.

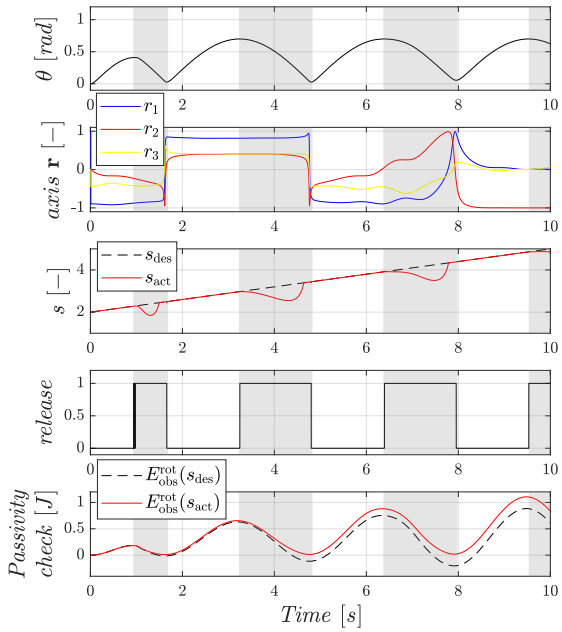

Fig. 6: Simulation of Method M1 with unitary variation of reference angle and axis $(\Theta, \mathbf{r})$, constantly increasing desired stiffness s_{des}, and $k_0{=}\frac{Nm}{rad}$: DDPA limits stiffness to s_{act} ensuring passivity with $E_{\text{obs}}^{\text{rot}}(s_{\text{act}}){>}0J$. The shaded areas mark release phases.

- *Applied stiffness:* The stiffness scaling s_{act} applied to the spatial spring is chosen as the minimum of s_{des} and s_{lim}. Still, a minimum stiffness s_{min} may be considered ($s_{\text{act}} = max(min(s_{\text{des}}, s_{\text{lim}}), s_{\text{min}})$) which may lead to a limitation of s_{act} during the pressing phase [11].

Note that further recommendations regarding stiffness variation during the pressing path, parametrization of s_{lim}, and consideration of energy dissipated by damping in E_{obs} are discussed in [11].

IV. Simulation

Fig. 6 to Fig. 7 present the results of SO(3) DDPA simulations with Method M1 and M2. No mechanical models of input device and robot were applied in the simulation and force

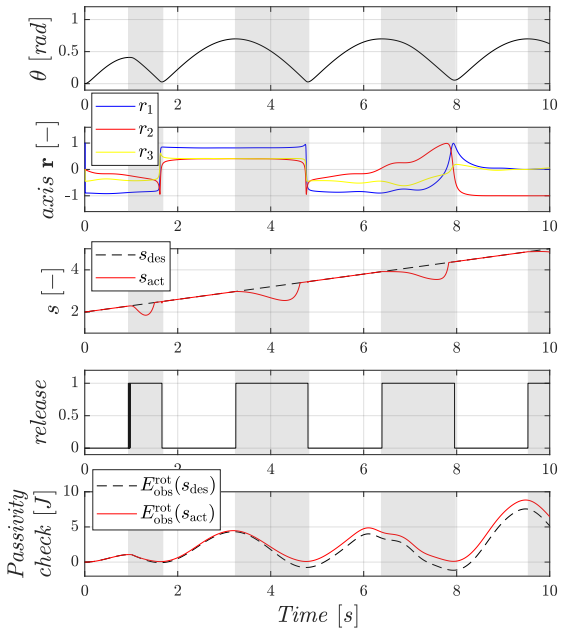

Fig. 7: Simulation of Method M2 with unitary variation of reference angle and axis $(\Theta, \mathbf{r})$, constantly increasing desired stiffness s_{des}, and $k_0{=}\frac{Nm}{rad}$: DDPA limits stiffness scaling to s_{act} ensuring passivity with $E_{\text{obs}}^{\text{rot}}(s_{\text{act}}){>}0J$. The shaded areas mark release phases.

feedback was neglected. The DDPA controlled spatial spring was fed an artificial input device pose x_I and the robot pose $x_R(k){=}x_I(k{-}T_d)$. Thus, the robot pose x_R matched the input device pose x_1 delayed by $T_d{=}120ms$ to simulate a dynamic behavior of the robot. The constantly increasing s_{des} was chosen to provoke active behavior of the stiffness variation. The angle Θ and axis $\mathbf{r}$ are derived from the input ${}^{\mathcal{D}}\mathbf{H}_{\mathcal{T}}$ to the spatial spring. In all simulations, deactivating the DDPA, it can be analyzed that the resulting observed energy $E_{\text{obs}}^{\text{rot}}(s_{\text{des}})$ becomes negative. This confirms the energy-generating behavior of the applied stiffness variation. It can be observed for both simulations that s_{act} (limited by the DDPA) leads to a passive system behavior: $E_{\text{obs}}^{\text{rot}}(s_{\text{act}}{\geq}0J)$.

In case of Method M1 (Fig. 6), a matrix with uniform diagonal entries ${}^{\mathcal{D}}\mathbf{K}_{\text{o}}{=}s_{\text{act}}k_0\mathbf{I}$ was applied which lead to overall lower energy values when compared to the subsequent experiments with method M2. A nonlinear spatial spring with the arbitrary positive definite and symmetric stiffness matrix

$$ {}^{\mathcal{D}}\mathbf{K}_{\text{o}} = s_{\text{act}}({}^{\mathcal{D}}\Theta_{\mathcal{T}}) \begin{bmatrix} 3 & 1 & 2 \\ 1 & 8 & 2 \\ 2 & 2 & 5 \end{bmatrix} \tag{20} $$

was applied in the experiment of Fig. 7. In the respective energy plots, the effect of the axis $\mathbf{r}$ due to the more complex stiffness matrix becomes obvious. Despite the major differences in the design of the spatial spring, the variation of s_{act} through the DDPA is very similar.

V. Experimental Evaluation

The following experiments were performed with the haptic input device lambda.7 developed by Force Dimension and a DLR light-weight robot as depicted in Fig. 8. The control was implemented in Matlab/Simulink and executed on a RT Linux system at 1kHz sampling rate. EMG measurements recorded with the Myo Armband were applied to set the desired stiffness. For more information on the stiffness estimation via EMG data, the reader is referred to [11]. For all experiments, the stiffness matrix was set to

$$ {}^{\mathcal{D}}\mathbf{K}_{\mathrm{o}} = s_{\mathrm{act}}({}^{\mathcal{D}}\Theta_{\mathcal{T}}) \begin{bmatrix} 0.3 & 0.01 & 0.03 \\ 0.01 & 1 & 0 \\ 0.03 & 0 & 1.5 \end{bmatrix}, $$

which was scaled by the DDPA-controlled scaling s_{act}. The deflection deadband was set to $\Theta_{\mathrm{db}} = 0.01\mathrm{rad}$. The first experiment shows that passivity is not guaranteed if DDPA is deactivated. The latter 6-DoF experiments evaluate the functionality of Method M2 in contact and free motion. Note that the EMG data was intentionally filtered only slightly to evaluate the robustness of the DDPA under harsher conditions.

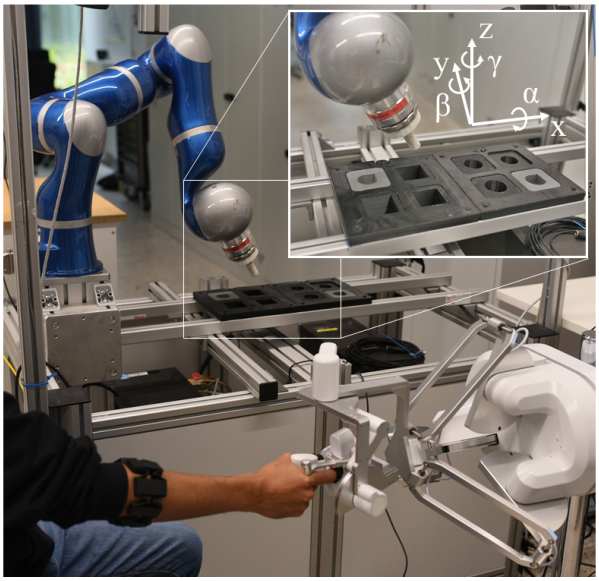

Fig. 8: Hardware setup: Light-weight robot (DLR), lambda.7 (Force Dimension), and Myo Armband (Thalmic Labs).

A. Deactivated DDPA

The first experiment presents an active behavior of variable stiffnesses in case of deactivated DDPA (see Fig. 9). The scaling s_{des} of the stiffness matrix had an offset of 10 ([-]) and could be increased to a value of 20 ([-]) by the normed EMG data. A wall contact was performed at t=$[15.6s, 21s]$. During the wall contact, the arm stiffness has been increased as visible from the plot of s_{des}. Although the stiffness has been decreased already during the release phase at t=$19s$, the observed energy attains negative values at t=$19.5s$ (shaded area). From the instant of the energy sign change until the end of the contact, the non-predictive time-domain approaches would attenuate the controller force completely, leading to a zero-stiffness phase. The same holds for the zero-crossing of the energies in the simulations of Section IV.

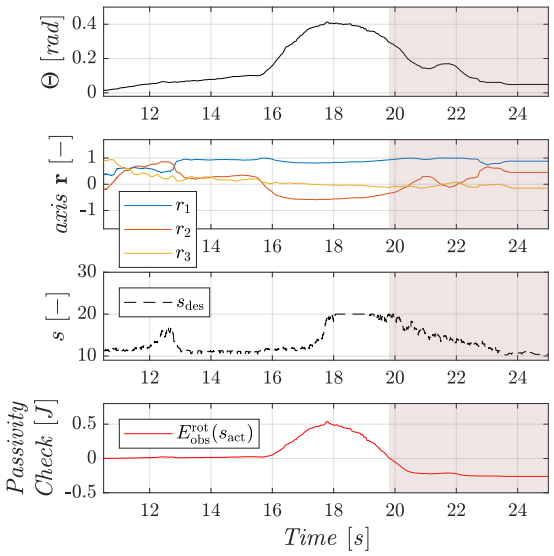

Fig. 9: Experiment with deactivated DDPA: Stiffness scaling is increased during pressing phase at $t = [17s, 18s]$ such that passivity is violated during release phase. The shaded area marks passivity violation.

B. Experiment with DDPA Method M2

The following experiments allow for the evaluation of the performance of DDPA Method M2. In both experiments, the robot is moved downwards in z-direction (not visualized) and then moves forward in x-direction into a wall contact. The scaling s_{des} of the stiffness matrix had an offset of 20 ([-]) and could be increased to a value of 40 ([-]) by the normed EMG data.

The plots of Fig. 10 present a free motion phase at t=$[40s, 51s]$ and two wall contacts (shaded area) at t=$[20.9s, 27.8s]$ and t=$[30.1s, 35s]$ respectively. The plot of axis $\mathbf{r}$ shows large variations indicating that the motion direction was varied in all rotational DoF. During the wall contacts, the spatial spring was mainly deflected in α as visible from Fig. 10b. Passivity is ensured although the stiffness was almost not adapted throughout the experiment by the DDPA. This is due to the fact that the desired stiffness was set via the Myo armband before the deflection of the spring and held constant during the deflection. The chosen deadband Θ_{db} leads to detection of several spring deflection phases, but the adaptation of stiffness through DDPA is not negatively affected. At $t = 11.5s$, the DDPA prevents a stiffness increase already during the pressing phase since the available energy is too low to guarantee the desired minimal stiffness scaling s_{min}. The torques τ_{des}=τ_α+τ_β+τ_γ and $\tau_{act} = \tau_{des}\frac{s_{act}}{s_{des}}$ present the minimal, indirect adaptation of torques analogous to s_{act}.

The second DDPA experiment (see Fig. 11) presents two wall contacts at t=$[10.7s, 17.6s]$ and t=$[21s, 29.5s]$ respectively. As observable from Fig. 11b, the spatial spring was again mainly deflected in α, whereas the orientation change in γ could be set by the robot without resistance. The first wall contact was initiated with high arm stiffness s_{des}. During the release phase, the stiffness was reduced. Since this presents a

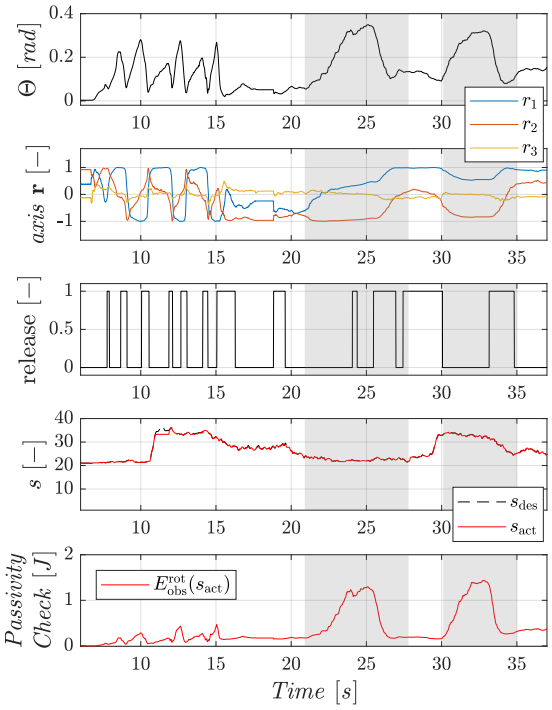

(a) Overview.

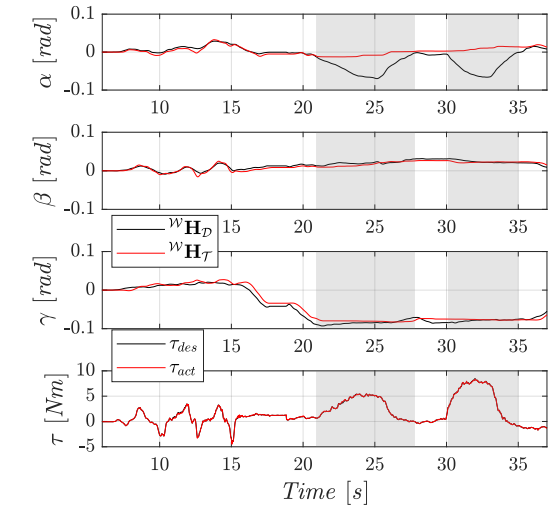

(b) Pose and Torques.

Fig. 10: Experiment involving EMG measurements and DDPA with free motion and two wall contacts: stiffness scaling is varied such that no adaptation of s_{act} is required to ensure passivity. The shaded areas mark wall contacts.

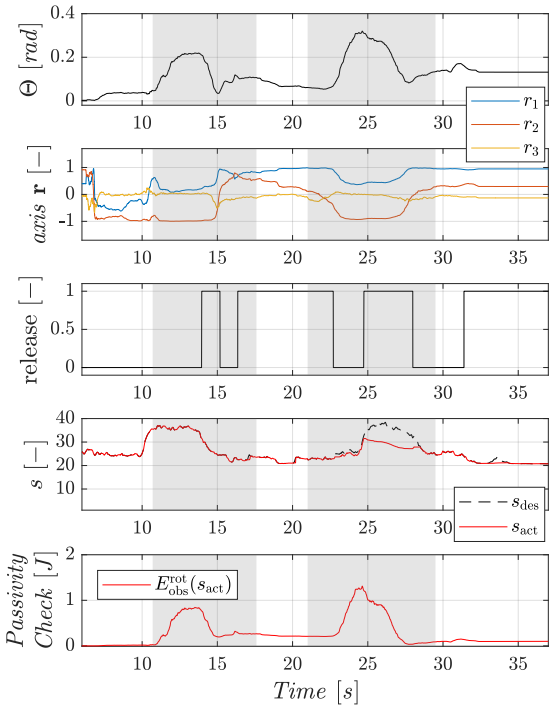

(a) Overview.

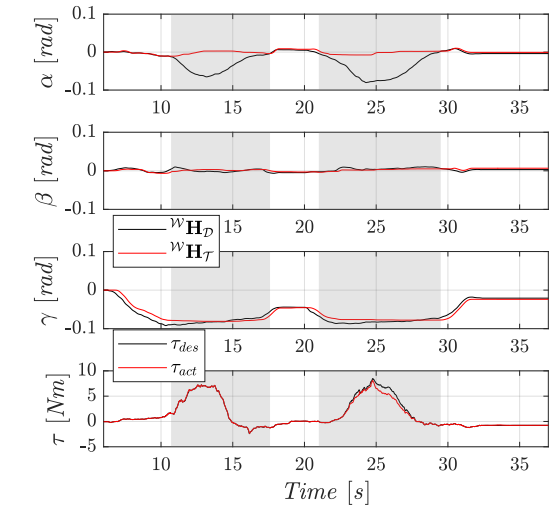

(b) Pose and Torques.

Fig. 11: Experiment involving EMG measurements and DDPA with free motion and two wall contacts: reducing stiffness during release phase of first wall contact does not require DDPA action. Adaptation of s_{act} during second wall contact since stiffness increased at comparably high deflection. The shaded areas mark wall contacts.

passive action, s_{act} did not need to be adapted by the DDPA to guarantee passivity. In contrast, the second wall contact was initiated with low stiffness. At $t = 24.6s$, the operator tries to increase the stiffness, but the DDPA limits the scaling to s_{act} to ensure passivity. Analogously, the torque τ_{des} is reduced to τ_{act}. It can be observed that the torques only need to be slightly varied to ensure passivity. Note that in case of non-predictive time-domain control, passivity violation would lead to a complete attenuation of the force and thus to a long zero-stiffness phase in this situation.

C. Discussion and Limitation

The DDPA operates with equal performance in rotational and translational DoF. It could be observed that due to the positive definiteness of the angle Θ of the angle-axis representation, the deadband Θ_{db} may need to be chosen comparably higher than in the translational DoF. The experiments with different complexity of rotations and interactions confirmed the DDPA ability to ensure passivity in case of arbitrary stiffness matrices for arbitrary unknown stiffness profiles.

The fact that the rotation matrix is scaled by one common DDPA scaling to ensure passivity may appear to be a limitation of the approach. Still, arbitrary stiffness matrices are feasible and since the rotations are energetically coupled, the solution should be sufficient for all relevant applications. In specific applications, terms coupling translations and rotations in the spatial spring may be relevant which cannot be handled by the DDPA so far. A solution to this is not obvious and remains for future work. The torque plots show that the DDPA requires only slight adaptation for the sake of passivity. Still, the limitation of the stiffness during the pressing phase may be reduced through more advanced approaches in future.

VI. Conclusion and Future work

This work introduced a 6-DoF extension of the deflection-domain passivity approach based on the angle-axis representation. Analogous to the 1-DoF DDPA, two scalar control references (observed energy and spring deflection) and a scalar control variable (limited stiffness) could be defined. The angle of the angle-axis representation was identified as a suitable deflection scalar. It was shown that the 1-DoF DDPA can be directly applied in case of diagonal stiffness with uniform diagonal entries. Furthermore, an extended DDPA solution for arbitrary stiffness matrices was developed and validated. The free motion and contact experiments confirmed the passivity of the approach. In future, the DDPA can be applied in 6-DoF time-domain controllers also to avoid sudden force attenuation through prescient stiffness attenuation.

Acknowledgment

The work was partially funded by the Bavarian Ministry of Economic Affairs, Regional Development and Energy, within the project SMiLE2gether (LABAY102). The research work was partially funded by the German Research Foundation (DFG, Deutsche Forschungsgemeinschaft) as part of Germany's Excellence Strategy – EXC 2050/1 – Project ID 390696704 – Cluster of Excellence "Centre for Tactile Internet with Human-in-the-Loop" (CeTI) of Technische Universität Dresden.

References

[1] M. Panzirsch, A. Pereira, H. Singh, B. Weber, E. Ferreira, A. Gherghescu, L. Hann, E. den Exter, F. van der Hulst, L. Gerdes *et al.*, "Exploring planet geology through force-feedback telemanipulation from orbit," *Science Robotics*, vol. 7, no. 65, p. eabl6307, 2022.

[2] M. Laghi, A. Ajoudani, M. G. Catalano, and A. Bicchi, "Unifying bilateral teleoperation and tele-impedance for enhanced user experience," *IJRR*, vol. 39, no. 4, pp. 514–539, 2020.

[3] F. Ferraguti, C. Secchi, and C. Fantuzzi, "A tank-based approach to impedance control with variable stiffness," in *ICRA*. IEEE, 2013, pp. 4948–4953.

[4] A. Dietrich, X. Wu, K. Bussmann, C. Ott, A. Albu-Schäffer, and S. Stramigioli, "Passive hierarchical impedance control via energy tanks," *IEEE RA Letters*, vol. 2, no. 2, pp. 522–529, 2016.

[5] Y. Michel, C. Ott, and D. Lee, "Passivity-based variable impedance control for redundant manipulators," in *IFAC World Congress (IFAC)*, 2020.

[6] N. Hogan, "Impedance control: An approach to manipulation," in *1984 American control conference*. IEEE, 1984, pp. 304–313.

[7] K. Kronander and A. Billard, "Stability considerations for variable impedance control," *IEEE Transactions on Robotics*, vol. 32, no. 5, pp. 1298–1305, 2016.

[8] T. Morita, H. Iwata, and S. Sugano, "Development of human symbiotic robot: Wendy," in *ICRA*, vol. 4. IEEE, 1999, pp. 3183–3188.

[9] J. W. Hurst, J. E. Chestnutt, and A. A. Rizzi, "An actuator with physically variable stiffness for highly dynamic legged locomotion," in *ICRA*, vol. 5. IEEE, 2004, pp. 4662–4667.

[10] S. Wolf, O. Eiberger, and G. Hirzinger, "The dlr fsj: Energy based design of a variable stiffness joint," in *2011 IEEE International Conference on Robotics and Automation*. IEEE, 2011, pp. 5082–5089.

[11] M. Panzirsch, M. Sierotowicz, R. Prakash, H. Singh, and C. Ott, "Deflection-domain passivity control of variable stiffnesses based on potential energy reference," *IEEE RA Letters*, vol. 7, no. 2, pp. 4440–4447, 2022.

[12] H. Singh, A. Jafari, and J.-H. Ryu, "Enhancing the force transparency of time domain passivity approach: Observer-based gradient controller," in *2019 International Conference on Robotics and Automation (ICRA)*. IEEE, 2019, pp. 1583–1589.

[13] H. Singh, M. Panzirsch, and J.-H. Ryu, "Preserving the physical coupling in teleoperation despite time delay through observer-based gradient control," *IFAC-PapersOnLine*, vol. 52, no. 18, pp. 25–30, 2019.

[14] M. Panzirsch, J.-H. Ryu, and M. Ferre, "Reducing the conservatism of the time domain passivity approach through consideration of energy reflection in delayed coupled network systems," *Mechatronics*, vol. 58, pp. 58–69, 2019.

[15] M. Panzirsch, H. Singh, X. Xu, A. Dietrich, T. Hulin, E. Steinbach, and A. Albu-Schaeffer, "Enhancing the force transparency of the energy-reflection based time domain passivity approach," *IEEE Transactions on Control of Network Systems*, vol. submitted, 2023.

[16] M. Panzirsch, H. Singh, and C. Ott, "The 6-dof implementation of the energy-reflection based time domain passivity approach with preservation of physical coupling behavior," *IEEE RA Letters*, vol. 5, no. 4, pp. 6756–6763, 2020.

[17] M. Rothammer and J.-H. Ryu, "Error-domain conservativity control to transparently increase the stability range of time-discretized controllers," in *ICRA*. IEEE, 2023, pp. 12 514–12 520.

[18] E. D. Fasse and J. F. Broenink, "A spatial impedance controller for robotic manipulation," *IEEE Transactions on Robotics and Automation*, vol. 13, no. 4, pp. 546–556, 1997.

[19] S. Stramigioli and V. Duindam, "Variable spatial springs for robot control applications." in *IROS*, 2001, pp. 1906–1911.

[20] O. Rodrigues, "Des lois géométriques qui régissent les déplacements d'un système solide dans l'espace, et de la variation des coordonnées provenant de ces déplacements considérés indépendamment des causes qui peuvent les produire," *Journal de mathématiques pures et appliquées*, vol. 5, pp. 380–440, 1840.

[21] S. Zhang and E. D. Fasse, "Spatial compliance modeling using a quaternion-based potential function method," *Multibody System Dynamics*, vol. 4, pp. 75–101, 2000.

[22] C. Ott, *Cartesian impedance control of redundant and flexible-joint robots*. Springer, 2008.